



# Physicochemical characterization and biological response of PDMS/CS/PVA/GEN semi-interpenetrating networks as a function of CS/PVA/GEN ratio for tissue engineering

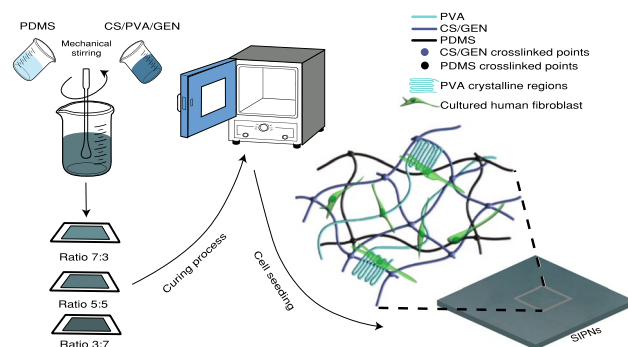
Jorge Alejandro Benítez-Martínez<sup>1,2</sup> · Itzel Marisol Garnica-Palafox<sup>1</sup> · Adriana Rodríguez-Hernández<sup>3</sup> · Daniel Pérez-Calixto<sup>3,4</sup> · Genaro Vázquez-Victorio<sup>3</sup> · Agileo Hernández-Gordillo<sup>1</sup> · Francisco Manuel Sánchez-Arévalo<sup>1</sup>

Received: 22 April 2023 / Accepted: 29 June 2023 / Published online: 15 July 2023  
© The Author(s) 2023

## Abstract

We demonstrated that the combination of poly(dimethylsiloxane) (PDMS) and a hybrid hydrogel based on chitosan/poly(vinyl alcohol)/genipin (CS/PVA/GEN)—with ratios 7:3 (SIPNs1), 5:5 (SIPNs2), and 3:7 (SIPNs3) (w/w)—were useful for obtaining semi-interpenetrated polymeric networks (SIPNs). These SIPNs successfully combined the PDMS's elasticity, the PVA's swelling capability, and the excellent biological response of CS and GEN. Noticing these features are desirable in materials intended for biomedical applications such as wound healing and tissue engineering. Through evaluating the influence of PDMS and CS/PVA/GEN hybrid hydrogel ratios on the physico-chemical, mechanical, and the response of seeded cells, we found contact angles between 55° and 75°, while the swelling percentage was enhanced up to three times concerning blank PDMS. Besides, the elastic moduli presented values between 1 and 1.6 MPa. The fibroblasts seeded on the tested semi-interpenetrating polymeric networks were viable, and no cytotoxic effects were found. The cells presented fusiform shapes indicating an excellent attachment to the material's surface. The highest cell densities were found for SIPNs1 and SIPNs2, suggesting that these compositions in a membrane shape could potentially be used in wound healing/dressing or as a scaffold for tissue engineering.

## Graphical abstract



**Keywords** Semi-interpenetrating polymeric networks · Poly(dimethylsiloxane) · Chitosan · Poly(vinyl alcohol) · Genipin

Jorge Alejandro Benítez-Martínez, Itzel Marisol Garnica-Palafox, Adriana Rodríguez-Hernández, Daniel Pérez Calixto, Genaro Vázquez-Victorio, Agileo Hernández-Gordillo, and Francisco Manuel Sánchez-Arévalo have contributed equally to this work.

Extended author information available on the last page of the article

## 1 Introduction

Chronic wounds are the main complication for those patients who suffer burns or patients with diabetics undergoing chronic pressure ulcers, among others [1–3]. The worldwide

statistics report that chronic wounds have become a significant global health issue. This health issue represents an incidence range between 2 and 6% for developed countries; however, the same health issue has a higher impact for underdeveloped countries showing an incidence of more than twofold times for developed countries [1, 4]. According to the medical protocols reported in the literature, the first step in treating a wound is immediate coverage to prevent infection and promote healing [5–7]. Then classical wound treatments could be applied. Among them, autografts, allografts, or xenografts are found. Regarding the use of classical wound treatments, two main complications exist: first, a limited availability of native skin from donors, and second, some of these treatments could produce antigenicity or even the risk of rejection and severe infections. To deal with these issues, some new materials and synthetic polymers, such as skin substitutes and hydrogels, have been recently raised for tissue regeneration and skin wound treatments [7–10].

Skin substitutes are biomaterials that can act as permanent skin replacements or temporary wound covers, accelerating their healing process [11]. Depending on their origin and components, they could be classified as synthetic or biological skin substitutes. Among the most used commercial skin substitutes, we found Integra, Biobrane, TransCyte, and Hyalomatrix. These brands present some advantages, such as their availability, size, and shape, to provide a physical barrier from bacteria [11–13]; reducing mortality and morbidity from scarring. Albeit they also have disadvantages, e.g., their high costs (\$3000–\$13,000 per 100 squared centimeter), the risk of disease transmission, immune rejection, infection due to fluid buildup or even multiple required surgeries [13–15]. Although there are many skin substitutes, neither fulfills all the features of an ideal skin substitute [9, 14]. That is why hydrogels have recently attracted the attention of scientific and medical communities to develop more effective materials and treatments for wound healing.

Hydrogels are three-dimensional macromolecular networks joined together by covalent bonds, ionic forces, hydrogen bonds, hydrophobic interactions, polymer crystallites, physical entanglements of various polymer chains, or a combination of them [10]. One of the main features of hydrogels is their absorption capability; thus, large amounts of liquid can be trapped within their structure. Two of the most widely polymers to form hydrogels are poly(vinyl alcohol) (PVA) and chitosan (CS). PVA is a nontoxic, synthetic polymer whose structure consists of a backbone of carbon atoms and pendant hydroxyl groups. Due to PVA's biocompatibility and a high swelling degree, it has been used in tissue engineering like cartilage replacements [16], bone scaffold [17], and drug delivery applications [18]. However, this polymer does not promote cell adhesion by itself. Therefore, combining it with a polysaccharide such as chitosan is usually done to overcome this drawback [19–21]. Chitosan is a natural

polymer obtained by the deacetylation of chitin under alkaline conditions. This natural polymer has advantages over others because it possesses anti-inflammatory, anti-fungal, anti-bacterial, anti-microbial, anti-coagulant, and hemostatic properties [22–24]. This set of properties provides a micro-environment that is suitable to promote rapid wound healing [25–27]. Noticing that its structure is similar to the structure of glycosaminoglycans present in the extracellular cell matrix (ECM), which benefits the cell adhesion and the proliferation response of the seeded cells [28].

Recently, some studies have been conducted on CS and PVA blends to understand the effect of chemical crosslinkers such as glutaraldehyde [29], epichlorohydrin [30], genipin [19, 20, 31]; however, still exists the need to enhance the physicochemical, mechanical, and biological responses of this hybrid hydrogel; particularly, towards wound healing and tissue engineering applications. In this sense, the genipin still is a good alternative as a crosslinker reagent because of its low cytotoxicity compared with other crosslinker reagents [19, 29, 30]. The mechanical response of CS/PVA/GEN could be tuned to obtain similar mechanical behavior to the human skin, remembering that it is an essential feature that must be found in a skin substitute [14, 32, 33]. To enhance the mechanical behavior, another polymer might be added to the CS/PVA/GEN blend. In this sense, the poly(dimethylsiloxane) (PDMS) can be considered because of its mechanical behavior and biocompatibility [34, 35]. The PDMS is a synthetic polymer that presents attributes such as non-immunogenicity, non-toxicity, good mechanical stability, and good gas permeability to be considered promising for skin substitutes; nevertheless, blank PDMS has poor cellular adhesion due to its hydrophobic behavior. During recent years, some efforts have been conducted to combine PDMS with PVA, e.g., Morales-Hurtado et al. reported the blend of PDMS with PVA crosslinked with glutaraldehyde [36] as a model to understand the human skin mechanical behavior; the main disadvantage of these kind of blends is focused on toxicity effects caused by glutaraldehyde [23, 37–39]. Further, in 2019, Chen et al. [40] combined PDMS with carboxyl chitosan. They found that this material had similar mechanical properties to the forearm skin, particularly the elastic modulus. In 2021, Semi-interpenetrating polymeric networks based in PDMS/CS/PVA crosslinked with genipin were successfully developed [1]. Here, the physicochemical and biological response of PDMS and CS/PVA/GEN 7:3 ratio were explored [1]. It is the only report in the literature concerning the PDMS/CS/PVA/GEN blend, and it is clear that more exhaustive research must be conducted to get a deep understanding of these semi-interpenetrating polymer networks (SIPNs). Therefore, the main purpose of this work was to explore the effects of the PDMS and CS/PVA/GEN ratios on their physicochemical, mechanical,

and biological responses to obtain semi-interpenetrating polymeric networks intended for wound dressing/healing and scaffolds for tissue engineering.

## 2 Materials and methods

### 2.1 Materials

The semi-interpenetrating polymeric networks were synthesized using synthetic and natural polymers. As synthetic polymers, poly(dimethylsiloxane) (PDMS Sylgard 184 kit from Dow Corning, USA) and poly(vinyl alcohol) (PVA), with a 99% degree of hydrolysis and a typical average molecular weight (Mw) of 89,000–98,000 g/mol, were used. Chitosan (CS) with a 75–85% degree of deacetylation and a medium-molecular weight (190,000–310,000 g/mol), was used as a natural polymer. Besides, analytical grade genipin (GEN) powder was utilized as a chemical crosslinking reagent. These chemicals were purchased from Sigma-Aldrich and used as received.

### 2.2 Semi-interpenetrating polymeric networks (SIPNs) preparation

Here, we present the preparation details regarding the three different polymeric blends used in this work. Notice that in Table 1, we show the composition of the blends with their respective labels to identify them further in the text and figures quickly.

The SIPNs were obtained in a membrane shape using the solvent casting method. For this, the polymer blend PDMS/CS/PVA/GEN was prepared in three stages. The first one involves the CS/PVA/GEN solution preparation. The second stage is regarding the PDMS mixture considering a 10:1 weight ratio. The third and final stage concerns the combination procedure in the different ratios (7:3, 5:5, and 3:7 w/w). Notice that the first number corresponds to the PDMS ratio, and the second corresponds to the CS/PVA/GEN blend ratio, as shown in Table 1).

**Table 1** Polymer blends' labels show composition and materials ratios (w/w) for further reference within the text and figures

Sample name	PDMS ratio	CS/PVA/GEN ratio
SIPNs1	7	3
SIPNs2	5	5
SIPNs3	3	7

### 2.2.1 Preparation of the CS/PVA/GEN solution

A 2.5% (w/v) chitosan solution was obtained by dissolving CS powder in a 1% (v/v) acetic acid solution. This solution was kept under magnetic stirring at room temperature for 24 h until reaching a homogeneous solution. Then the PVA solution (10% (w/v)) was prepared by dissolving PVA powder in deionized water under magnetic stirring at 80 °C for 1 h. Afterward, it was cooled at room temperature for 1 h under magnetic stirring. CS and PVA polymeric solutions were mixed at a 3:1 volume ratio. This ratio promotes the miscibility and formation of a polymeric network. Therefore, solid intermolecular interactions are obtained, yielding CS/PVA blends with excellent chemical and physical properties, as was reported in the literature [41–43]. The CS/PVA blend was magnetically stirred for 1 h at room temperature. Subsequently, a genipin solution of 0.42% (w/v) was slowly incorporated into CS/PVA mixture and continued in magnetic stirring for 1 more h.

### 2.2.2 Preparation of the PDMS/CS/PVA/GEN solution

Once the preparation of the CS/PVA/GEN polymeric blend was finished, the PDMS Sylgard 184 kit was used to mix parts A (elastomer base) and B (curing reagent) in a 10:1 weight ratio. The elastomer base and its curing reagent were mechanically stirred for 5 min. Subsequently, the PDMS and CS/PVA/GEN were mixed with 7:3, 5:5, and 3:7 weight ratios. Thus, we obtained the blends labeled SIPNs1, SIPNs2, and SIPNs3, respectively, as shown in Table 1.

### 2.3 Fabrication of the membranes

Once the blend of each SIPNs was prepared, they were centrifuged for 10 min at 5000 rpm to eliminate air bubbles trapped in the polymeric solutions. Then, each solution was poured into 3D PLA-printed squared frames fixed on a polypropylene mat with double-sided adhesive tape. Notice that the 3D printed frames were designed in a CAD environment and printed with a Flash Forge Creator Pro 3D printer. We use a printing speed of 60 mm s<sup>-1</sup>, an extruder temperature of 200 °C, and a platform temperature of 50 °C. The dimensions of the frames were 60 × 60 mm and 0.5 mm in thickness. Once the blend was poured, it was spread using the "doctor blade method" to cover the frame entirely and uniformly. Then, each filled mold with the SIPNs was cured at 55 °C for 24 h to obtain the membranes. Finally, they were detached and stored in a desiccator until testing.

### 2.4 Physical and chemical characterization

The purpose of physicochemical characterization centers on correlating the changes in the chemical and physical

properties due to the different PDMS and CS/PVA/GEN weight ratios present in the SIPNs. Mainly, we focused on surface and volume hydrophilicity through contact angle measurements and swelling capacity, respectively; Fourier transform infrared (FT-IR) spectroscopy tracked the possible changes in the chemical structure of the SIPNs; atomic force microscopy (AFM) was used to measure the roughness of the SIPNs; the thermal stability of the SIPNs was measured by thermogravimetric analysis (TGA); while the mechanical behavior of the SIPNs—in membrane shape—was tested by uniaxial and biaxial tensile tests. Details of physicochemical assays will be further presented.

#### 2.4.1 Surface and volume hydrophilicity

Contact angle measurements were performed in triplicate to evaluate the surface hydrophilicity of SIPNs. In this case, the contact angles of water on the surface of the SIPNs were measured at room temperature using the sessile drop method. Hence, a drop of deionized water (5  $\mu\text{L}$ ) was cautiously placed onto the surface of each sample. Then, images were recorded by a CCD camera and saved on a PC through a virtual instrument programmed in LabView. The images were analyzed to measure the contact angle between the drop edge and the material surface on both sides of the drop. These angles were measured by digital image analysis through Vision Assistant 2016 software and further averaged. Hence, the contact angle average and their corresponding standard deviation were obtained. Notice that the SIPNs were previously hydrated in deionized water.

The volume hydrophilicity was evaluated using the swelling test in triplicate. Three circular samples of 12 mm in diameter from each SIPNs were cut. Thus, the SIPNs were weighed in a dry state and subsequently immersed in deionized water at room temperature. The swelling ratio (%S) was calculated with the typical equation reported in the literature [19] and following the procedure previously reported by Benítez-Martínez et al. [1].

#### 2.4.2 Chemical interaction of the SIPNs analyzed by FT-IR spectroscopy

The chemical interaction of the SIPNs were studied using FT-IR ATR spectroscopy (attenuated total reflectance) considering the following parameters: wavenumber ranges from 4000 to 400  $\text{cm}^{-1}$ , resolution of 2  $\text{cm}^{-1}$ , and 32 scans (Nicolet 6700, Thermo Fisher Scientific, Waltham, MA, USA). The main vibration bands were identified and associated with the PDMS, CS, PVA, and GEN chemical groups. The FT-IR measurements were carried out in triplicate in circular samples of 12 mm of diameter and thickness ranging between 300 and 500 microns.

#### 2.4.3 Surface morphology of the SIPNs is characterized by atomic force microscopy (AFM)

A Naio-AFM atomic force microscope (from Nanosurf, Liestal, Switzerland) was used to observe the surface morphology of the SIPNs. The images were registered using a commercial silicon probe ContAl-G with an aluminum reflective coating (BudgetSensors, Sofia, Bulgaria). The tip's radius was 10 nm with a spring constant of 0.2  $\text{N m}^{-1}$ , and it was used a resonance frequency of 13 kHz. The data acquisition and further analysis were performed with Naio Control Software 3.10 (Nanosurf, Liestal, Switzerland). These measurements were done in triplicate, at room temperature, in air, with dry samples, and under static force operating mode. The samples with a size of 12 mm in diameter were added to an AFM metal specimen disc with double-sided conductive carbon adhesive tape and placed onto the sample stage for measurement. The scanning size was 5  $\times$  5 microns for all measurements. In our case, the root mean square roughness (Sq) was calculated over the full scanned area.

#### 2.4.4 Thermal stability and crystallinity of the SIPNs

The thermal stability and decomposition rate were carried out for the SIPNs by thermogravimetric analysis (TGA). A thermogravimetric balance Q5000 IR (from TA Instruments, New Castle, DE, USA) was used. These measurements were performed by triplicate, under a nitrogen atmosphere and a heating rate of 10  $^{\circ}\text{C min}^{-1}$  from room temperature to 700  $^{\circ}\text{C}$ . The TGA data were analyzed using the TA Instruments Universal Analysis 2000 software (TA Instruments, New Castle, DE, USA).

The crystallinity of the SIPNs was determined by X-ray diffraction and by applying the cut and weight method [19, 21, 44]. We used a diffractometer Bruker D8 Advanced (Billerica, MA, USA) operating at 45 kV with Ni-filtered  $\text{CuK}\alpha 1$  radiation ( $\lambda = 1.5406 \text{ \AA}$ ). The diffraction patterns were recorded over the  $2\theta$  range of 5–70  $^{\circ}\text{C}$  with a 0.4  $^{\circ}\text{C min}^{-1}$  scan rate.

### 2.5 Mechanical behavior of the SIPNs by uniaxial and biaxial tensile tests

#### 2.5.1 Uniaxial tensile test

The uniaxial tensile test was carried out at room temperature in a hydrated fashion by triplicate. Thus, the membranes were previously hydrated until reaching equilibrium at swelling. The tensile specimens were cut according to the ASTM D1708 standard. Then the thicknesses and widths of the samples were measured using a micrometer (model MDC-1-SXF, Mitutoyo, Corp., Kawasaki, Japan) and a digital caliper (CD-6 CS, Mitutoyo, Mitutoyo, Corp., Kawasaki,

Japan), respectively. The previous measures were utilized to calculate the cross-section area for the uniaxial tensile test specimens. The uniaxial tensile test was conducted using a costume-designed device applying a strain rate of 0.16 mm/s according to the ASTM D882 standard. Thus, the displacement and the force data were acquired through National Instruments boards and a virtual instrument specially programmed in LabVIEW. From the registered data, the stress curves as a function of the elongation ratio were obtained for the SIPNs. The experimental data of these curves were fitted using a third-order Mooney–Rivlin model [45, 46]:

$$\sigma = 2C_{10}\left(\lambda - \frac{1}{\lambda^2}\right) + \left(2C_{01}\left(\lambda - \frac{1}{\lambda^3}\right)\right) + \left(6C_{11}\left(\lambda^2 - \lambda - 1 + \frac{1}{\lambda^2} + \frac{1}{\lambda^3} - \frac{1}{\lambda^4}\right)\right), \quad (1)$$

where  $\sigma$  is the engineering stress, in Pa,  $\lambda$  is the elongation ratio;  $C_{10}$ ,  $C_{01}$ , and  $C_{11}$  are coefficients that define the shape of the stress-elongation ratio curve. Thus, according to the literature, the elastic modulus could be calculated as the limit when  $\lambda \rightarrow 1$  of the partial derivative of the stress with respect to the elongation ratio:  $E = \lim_{\lambda \rightarrow 1} \frac{\partial \sigma}{\partial \lambda}$  [47]. Hence, considering a third-order Mooney–Rivlin model, the elastic modulus of the SIPNs was calculated as  $E = 6(C_{01} + C_{10})$ .

### 2.5.2 Biaxial tensile test by indentation

In the case of biaxial tensile tests, the membranes were hydrated as well as previously described. These mechanical assays were conducted by indentation in triplicate according to the methodology described by Garnica-Palafox et al. [48]. Thus, each membrane of 60 squared millimeters was firmly clamped between the plates of the sample holder of the biaxial mechanical tester, avoiding wrinkles or any damage on the surface of the mounted SIPNs. The hydrated SIPNs samples were indented in a controlled fashion at a constant rate of 0.16 mm/s at room temperature. The force ( $w$ ) and displacement ( $\delta$ ) data were recorded during the assay for further analysis. Notice that the elastic modulus of SIPNs was calculated according to the model reported by Garnica-Palafox et al. [48]:

$$\frac{6w}{EhR} = \frac{27\pi}{8\left(\frac{a}{R}\right)^{\frac{9}{4}}}\left(\frac{\delta}{R}\right)^3, \quad (2)$$

where ( $h$ ) is the membrane thickness, ( $R$ ) the indenter radius, ( $a$ ) the sample holder radius, ( $w$ ) the central applied load, ( $\delta$ ) corresponds to the central displacement, and  $E$  is the elastic modulus, thereby, the elastic modulus was determined as the slope of the linear section of the load–deflection curve  $6w$  versus  $\frac{27\pi}{8\left(\frac{a}{R}\right)^{\frac{9}{4}}}\left(\frac{\delta}{R}\right)^3 hR$ .

## 2.6 In vitro viability and cytotoxicity behavior of the SIPNs

### 2.6.1 Cell culturing

Immortalized human fibroblasts, namely BJ cell line (ATTC CRL-2522), were defrosted by placing the cryovials in water at 37 °C for 2 min. Once the fibroblasts were defrosted, the medium was removed. Then, the cells were disaggregated by pipetting and transferred to a Petri dish. Finally, the cells within the Petri dish were maintained in Dulbecco's Modified Eagle's Medium (DMEM) high glucose complemented with 10% fetal bovine serum (FBS), GlutaMAX 1X, and Antibiotic-Antimycotic 1X at 37 °C, 5% de CO<sub>2</sub>. The culture medium was replaced every 2 days until reaching confluence. All these reagents were purchased from Gibco (Thermo Fisher Scientific, Massachusetts, USA) and used as received.

### 2.6.2 Fabrication and preparation of samples for in vitro viability and cytotoxicity assays

Circular glass coverslips were coated with the SIPNs, following the same procedure of the membranes fabrication. This procedure assures good adhesion conditions between the SIPNs and the coverslips, avoiding free floating matrices/tension-free environment that could affect the cells' behavior [49]. Besides, it allows better-controlled conditions for cell seeding and their subsequent observation by epifluorescence microscopy. The coatings consider thicknesses ranging from about a couple of hundred microns and diameters of 17 mm. Blank and coated coverslips were placed into 12-well cell culture plates to be sterilized. Then, they were washed five times with 1 ml of ethanol 70% v/v (previously sterilized with 0.22  $\mu$ m filter), and five times with Dulbecco's Phosphate-Buffered Saline (DPBS) sterile 1X (Sigma-Aldrich). Then, each sample was incubated with 25  $\mu$ g/ml of fibronectin for 10 min. After this time, the fibronectin was removed, and the samples were washed with deionized water (previously sterilized with 0.22  $\mu$ m filter). Subsequently, the samples within the 12-well cell culture plates were dried at room temperature in sterile conditions for 40 min. Finally, they were sealed and stored overnight at 4 °C until cell seeding.

### 2.6.3 Cell seeding

The cultured cells in the Petri dishes were suspended by trypsin and seeded onto the SIPNs and an uncoated glass coverslip as control. The cellular density was  $5 \times 10^4$  cells per well. The uncoated and coated coverslips—with the

adhered cells—were cultured for 48 h at 37 °C and 5% of CO<sub>2</sub>; subsequently, the in vitro viability and cytotoxicity assays were performed.

### 2.6.4 In vitro viability and cytotoxicity assays

The viability and cytotoxicity responses of the adhered cells on the SIPNs were evaluated through a live/dead assay using calcein-AM/propidium iodide (PI). Each sample was washed with 1 ml of serum-free cell culture medium (DMEM high glucose, GlutaMAX 1X, and Antibiotic-Antimycotic 1X). Then, the samples were incubated with 1 μM of calcein-AM (Molecular Probes, ThermoFisher Scientific) and 5 μM of propidium iodide (ThermoFisher Scientific) in 1 ml of medium without serum for 15 min at 37 °C; After 15 min, the medium was aspirated and replaced by 1 ml more. Immediately, five images of each sample were captured in an epifluorescence microscope (Thunder, Leica, Wetzlar, Germany) using a 10X objective lens. All the images were saved and subsequently analyzed with Cell Profiler software. Thus, the cells were counted, and their main morphological features were evaluated as well. Notice the uncoated coverslips were used as control material for normal cell spreading, and these assays were done in triplicate.

## 3 Results and discussion

The semi-interpenetrating polymeric networks were successfully synthesized using three different weight ratios of PDMS and CS/PVA/GEN polymer blends, as described in Table 1. These SIPNs were obtained in a square membrane shape of 60 mm by the side. The thicknesses of the membranes were  $453 \pm 80$ ,  $376 \pm 52$ , and  $250 \pm 30$  microns for SIPNs1, SIPNs2, and SIPNs3, respectively (See Fig. 1a). We found a volume change after evaporating the solvents: 25% for SIPNs2 and 50% for SIPNs3 blends, compared with the SIPNs1 blend, which was 10%. Thus, SIPNs2 and SIPNs3 resulted in thinner membranes even using the same quantity of dissolution for their fabrication. A first visual inspection of all membranes revealed a whitish-light blue color—see inset in the lower right corner of Fig. 1b–d. The light blue color is mainly due to the crosslinking reaction between GEN and the primary amines of CS in the presence of oxygen [29, 50], while the whitish color is attributable to the presence of the PDMS in the SIPNs. Notice that our SIPNs were integrated by combining three polymers, PDMS, CS, and PVA. The PDMS, and CS were crosslinked by separately with their respective chemical reagents. The linear chains of PVA remain entangled between the PDMS and CS-GEN polymeric networks, satisfying the definition of SIPNs reported in the literature [51–53]. The obtained membranes were carefully inspected and selected for further

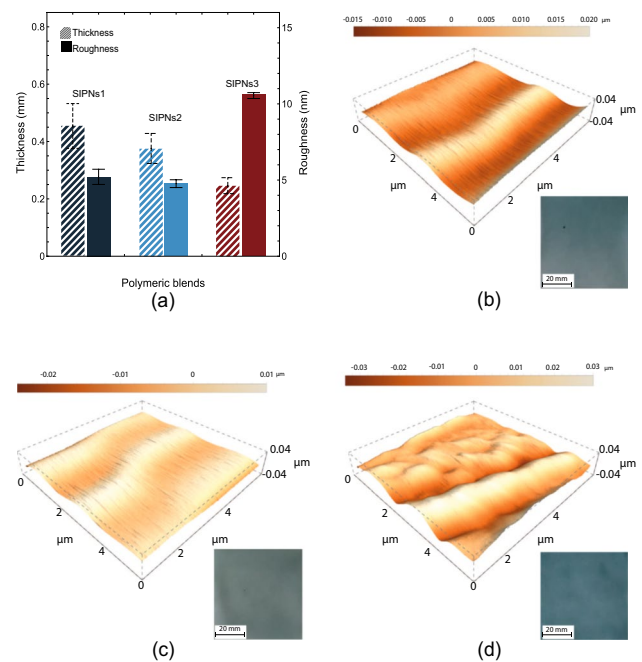


**Fig. 1** Morphological features of the SIPNs in membrane shape. **a** Average values and standard deviation of roughness and thickness of the synthesized membranes, **b** images of SIPNs1 obtained by AFM and optical microscopy, **c** images of SIPNs2 obtained by AFM and optical microscopy, **d** images of SIPNs3 obtained by AFM and optical microscopy

experiments. Hence, fabrication defects such as air bubbles, holes, and/or changes in thickness, among others, were avoided.

### 3.1 Surface topology

Figure 1b–d depicts representative images of the surface of the SIPNs measured by atomic force microscopy (AFM). From these images, the Root Mean Squared (RMS) roughness (Sq) for each SIPNs were determined using Nao control software from Nanosurf. Our results show that the Sq average values for SIPNs1, SIPNs2, and SIPNs3 were  $5.2 \pm 0.5$ ,  $4.8 \pm 0.2$ , and  $10.6 \pm 0.1$  nm, respectively, as shown in Fig. 1a. The Sq average values for our SIPNs agreed concerning those roughness values for PDMS [54–56] and CS/PVA/GEN [31] reported in the literature by the other authors. Moreover, our results suggest that the surface topology of the SIPNs smooths by increasing the proportion of CS/PVA/GEN to the blend until it reaches a 1:1 weight ratio with respect to the PDMS (Fig. 1b, c). If the CS/PVA/GEN ratio becomes greater than the PDMS ratio, the roughness will tend to increase, as observed in Fig. 1d. This might be due to the formation of fibrillar structures, which are associated with the folding of PVA polymeric chains [31] influencing the roughness of the SIPNs. Notice that the roughness

might influence other physical properties of the SIPNs, such as contact angle, swelling response, and even crystallinity. Previous studies have demonstrated that random surface roughness reduction positively affects cell adhesion, spreading, and proliferation of human skin fibroblasts [57–59], and human osteoblasts [60, 61].

### 3.2 Surface and volume hydrophilicity

Figure 2a presents the contact angle average values and their respective standard deviations that exhibited the SIPNs in contact with a drop of deionized water. These values were  $67.7^\circ \pm 2.1^\circ$ ,  $66.5^\circ \pm 2.1^\circ$ , and  $65.3^\circ \pm 2.4^\circ$  for SIPNs1, SIPNs2, and SIPNs3, respectively. According to Gupta et al. and Garnica-Palafox et al., contact angles between  $55^\circ$  and  $75^\circ$  are suitable for the adhesion of human fibroblast [31, 62].

Figure 2b shows the swelling kinetics of the SIPNs; here, the deionized water absorption percentage as a function of time is observed for each SIPNs. As it can be seen, after 16 days, the reached swelling ratios at equilibrium were:  $3.7 \pm 0.1\%$ ,  $15.3 \pm 0.2\%$ , and  $15.7 \pm 0.1\%$  for SIPNs1, SIPNs2, and SIPNs3, respectively. According to the literature, PDMS presents a low swelling ratio below 1% [63]. However, by adding the CS/PVA/GEN

to PDMS, we enhance its volume hydrophilicity almost 4-fold, 15-fold, and 16-fold times for SIPNs1, SIPNs2, and SIPNs3, respectively. Regarding the velocity of the swelling behavior, we found the fastest swelling rate during the first day; the values were  $3.1 \pm 0.3\%$ ,  $5.9 \pm 0.2\%$ , and  $11.0 \pm 0.6\%$  for SIPNs1, SIPNs2, and SIPNs3, respectively; beyond this time, the swelling rate was slow until equilibrium was reached.

### 3.3 Chemical interaction of SIPNs

The chemical interaction between the polymeric chains in the SIPNs was analyzed by FT-IR spectroscopy. The FT-IR spectra of all the studied SIPNs membranes, in dry and wet conditions, are shown in Fig. 2c, d. Our FT-IR results revealed that increasing the CS/PVA/GEN proportion in the SIPNs, produced a change of the transmittance percentage in the band at  $3700\text{--}3000\text{ cm}^{-1}$ . It was expected because this band is related to the N–H/O–H stretching vibration modes of chitosan and PVA [19, 31, 48, 64] presented in the CS/PVA/GEN blend. These bands are also related to the inter- and intramolecular hydrogen bonds due to the interaction between CS and PVA [21, 65]. The next band was observed between  $2960$  and  $2900\text{ cm}^{-1}$ ; it corresponds to the symmetric and asymmetric stretching vibrations of methyl groups C–H<sub>3</sub> bonds in the PDMS. In addition, in this same band are located the vibrations of the C–H groups ( $2930$  and  $2900\text{ cm}^{-1}$ ), which are present in both the chitosan and PVA components [1, 64]. The stretching vibration mode of the C=O bonds in the acetylated units of CS was detected between  $1680$  and  $1600\text{ cm}^{-1}$ . Likewise, between  $1600$  and  $1500\text{ cm}^{-1}$  were observed the bending vibration mode of the N–H bonds and the stretching vibration mode of the C–N bonds belonging to the amine and amide II in CS. The formation of heterocyclic amines due to the reaction of CS and GEN by the opening of the GEN dihydropyran ring was detected at  $1380\text{ cm}^{-1}$  [31]. The bands associated with Si–CH<sub>3</sub> bonds in the PDMS were detected at  $1257$  and  $785\text{ cm}^{-1}$  [66]. Finally, the band between  $1100$  and  $1000\text{ cm}^{-1}$  corresponds to the stretching vibration of Si–O, Si–O–Si, and Si–O–C bonds, because of the presence of PDMS in the SIPNs [67].

Figure 2d shows the FT-IR spectra of the SIPNs after 16 days in swelling (i.e. at swelling equilibrium state). Here, we observed a significant change in the bands between  $3700\text{--}3000\text{ cm}^{-1}$  and  $1700\text{--}1600\text{ cm}^{-1}$  for hydrated SIPNs, which is due to water's affinity with the N–H/O–H groups present in PVA and CS [36, 68]. This result agrees with the swelling results and demonstrates that the presence of hydroxyl groups in the CS/PVA/GEN blend improves the

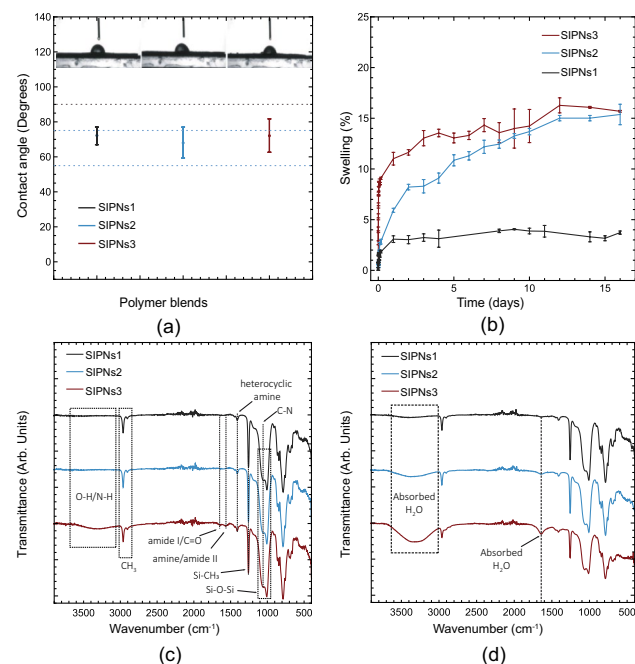


**Fig. 2** Surface and volume hydrophilicity responses of the SIPNs. **a** Contact angle average values and their corresponding standard deviations for each SIPNs, **b** swelling behavior as a function of time for each SIPNs, **c** representative FT-IR spectra under dry conditions for the SIPNs, **d** representative FT-IR spectra under wet conditions after 16 days of swelling for the SIPNs

volume hydrophilicity of those SIPNs with a higher CS/PVA/GEN volume.

### 3.4 Thermal stability, crystallinity, and mechanical behavior

Figure 3a depicts the thermal stability of all SIPNs throughout the TGA representative curves and their derivative thermogravimetric analysis (DTGA). The DTGA indicates the degradation process occurs in three main stages. From room temperature to 230 °C, all SIPNs were stable. Here, just a minimum weight loss (0.5–1.0%) was observed due to water evaporation. Higher water evaporation was present in SIPNs3, which is consistent with its swelling ratio; more swelling ratio implies more water to be evaporated. The first degradation stage occurred between 240 and 380 °C. It is owing to the dehydration of the saccharide rings of chitosan and the degradation of its acetylated and deacetylated units [26, 69]. In this stage, SIPNs1 and SIPNs2 registered a weight loss of  $4.8 \pm 0.14\%$ , meanwhile, the weight loss of SIPNs3 was  $8.19 \pm 0.44\%$ . The second stage of degradation was observed from 380 to 460 °C. Here, the SIPNs1 and SIPNs2 presented a  $5.39 \pm 0.63\%$  and  $5.51 \pm 0.05\%$  of weight loss; meanwhile, the SIPNs3 was  $6.52 \pm 0.12\%$ . This weight loss was mainly due to the degradation of the backbone of PVA [26, 69].

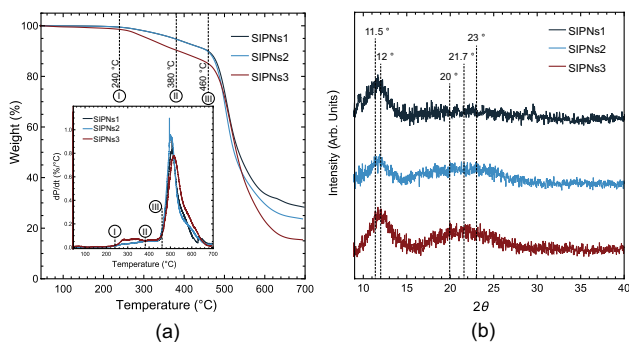
The third stage of degradation, located between 400 and 600 °C, owing to the depolymerization of PDMS to produce cyclic oligomers [70, 71]. At this temperature range, the weight loss for SIPNs1, SIPNs2, and SIPNs3 were  $61.1 \pm 2.6\%$ ,  $55.9 \pm 7.7\%$ , and  $66.7 \pm 6.8\%$ , respectively. Beyond 600 °C residual weights of  $28.3 \pm 3.2\%$ ,  $33.2 \pm 7.7\%$ , and  $17.4 \pm 7.3\%$  were observed for SIPNs1, SIPNs2, and SIPNs3, respectively.

Our TGA results demonstrated that all SIPNs are thermally stable from room temperature to 230 °C; therefore, sterilization treatments that involve a maximum temperature

of 160 °C [72] could be applied to SIPNs, avoiding any thermal degradation issue. Notice that sterilization treatments are essential for further uses of the SIPNs in biological/medical applications.

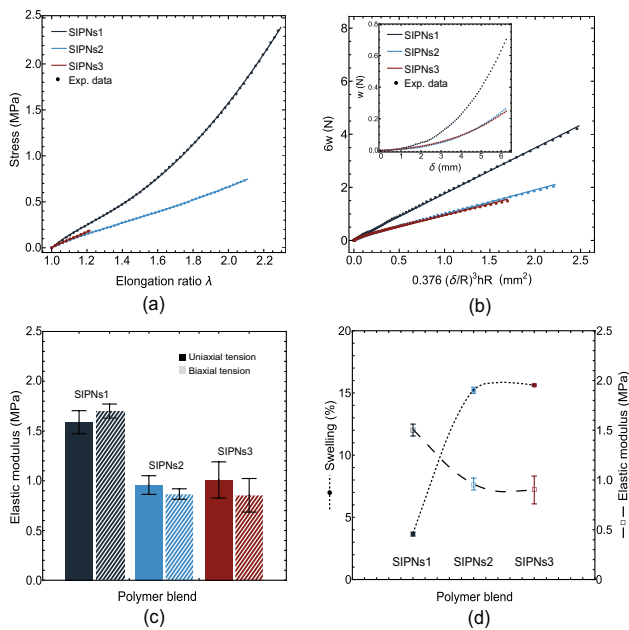
Figure 3b shows the X-ray patterns of all SIPNs. As can be seen, our SIPNs have a semi-crystalline state. Hence, the peak at  $11.5^\circ$  corresponds to the tetragonal unit cell of the PDMS' crystalline phase; this semi-crystalline nature of PDMS has been previously reported in the literature [34, 73–76]. Besides, the characteristic peaks of chitosan were located at  $20^\circ$  and  $21.7^\circ$ . These peaks correspond, respectively, to planes (200) and (201) of its orthorhombic crystalline phase [77–81]. Finally, the peaks of the monoclinic unit cell of the PVA's crystalline phase were present at  $12^\circ$  (corresponding to the (100) plane), at  $20^\circ$  (related to the (101) plane), and at  $23^\circ$  (corresponding to the (200) plane) [19, 82]. Notice that the diffraction intensity of the PMDS hides the CS and PVA peaks. The percentage of crystallinity of the SIPNs were  $37 \pm 4\%$ ,  $51 \pm 3\%$ , and  $59 \pm 3\%$  for the SIPNs1, SIPNs2, and SIPNs3, respectively. Here, it is observed that crystallinity increased 1.38- and 1.59-fold for SIPNs2 and SIPNs3, respectively, compared with SIPNs1. These results are consistent with the roughness results previously presented in Fig. 1. As mentioned before, the PVA tends to form fibrillar structures by folding polymer chains, increasing the roughness. Thus, the SIPNs with a higher amount of PVA presented greater surface roughness and, therefore, higher crystallinity.

Figure 4a depicts the mechanical responses of the SIPNs under uniaxial tensile loads. Notice that these assays were carried out with the SIPNs previously hydrated in deionized water until equilibrium was reached. Their representative curves of stress as a function of the elongation ratio are shown here. As it can be seen, the SIPNs exhibited a non-linear mechanical response, which is attributed to the rearrangement of the polymeric chains during the tensile test. Thus, the polymeric chains pass from an initial configuration—where the chains are randomly entangled—to a deformed configuration, where the chains are aligned in the direction of the applied load. From these stress-elongation ratio curves, the elastic modulus of each SIPNs was calculated through a three-parameters Mooney–Rivlin model using a non-linear fitting (continuous line), as it was previously described. The obtained values of the elastic moduli were  $1.59 \pm 0.11$  MPa,  $0.96 \pm 0.05$  MPa, and  $1.01 \pm 0.20$  MPa for SIPNs1, SIPNs2, and SIPNs3, respectively. From this result, we observed that a high content of PDMS within the SIPNs will aid in getting higher elastic moduli. Regarding the elongation ratio, we found that the SIPNs1 reached an average maximum elongation ratio of  $2.22 \pm 0.14$  with an associated ultimate tensile stress (UTS) of  $1.98 \pm 0.38$  MPa; the SIPNs2 presented an average elongation ratio of  $2.03 \pm 0.22$  and an average UTS of  $0.69 \pm 0.19$  MPa; finally, in



**Fig. 3** Thermal behavior and crystallinity percentage of the SIPNs. **a** Thermal stability of the SIPNs by TGA; the inset shows the DTGA of the SIPNs, **b** X-ray patterns showing the semi-crystallinity curves of the SIPNs





**Fig. 4** Mechanical characterization of each SIPNs. **a** Representative stress vs. elongation ratio curves under uniaxial tension and fitting using Mooney–Rivlin’s model (solid lines), **b** representative load–deflection curve and linear fitting (solid lines), **c** elastic moduli of the SIPNs obtained by uniaxial and biaxial tensions, **d** comparison of the behavior between swelling and elastic modulus of the SIPNs

the SIPNs3, we observed an average elongation ratio of  $1.27 \pm 0.07$  and an average UTS of  $0.23 \pm 0.06$  MPa. Considering the average values of the elongation ratio and UTS of SIPNs1 as a reference, we found a variation for the elongation ratio of 1.09 and 1.74 times for SIPNs2 and SIPNs3, respectively. Regarding the UTS we also found a variation of 2.86 and 8.6 times for SIPNs2 and SIPNs3, with respect to the UTS value of SIPNs1. Thus, SIPNs2 and SIPNs3 significantly reduce their mechanical response with respect to SIPNs1; it is due to the elasticity and strength that the content of PDMS provides to the SIPNs; thus, less content of PDMS lowers the mechanical response.

For the case of biaxial stress experiments, the non-linear response of the force vs. displacement data (see inset Fig. 4b) were processed using the model and methodology proposed by Garnica-Palafox et al. [48]. From the indentation data, the load–deflection curve was obtained using Eq. 2 and considering  $a/R = 5$ . It yield us to obtain  $6w$  as a function of  $0.376 \left( \frac{\delta}{R} \right)^3 hR$  curves, for each SIPNs, as shown in Fig. 4b. According to the model reported by Garnica-Palafox et al. [48], the slope of the linear section of this curve represents the elastic modulus of the SIPNs. As a result, we found average values of elastic moduli of  $1.69 \pm 0.07$  MPa,  $0.86 \pm 0.06$  MPa, and  $0.85 \pm 0.17$  MPa for SIPNs1, SIPNs2, and SIPNs3, respectively. Figure 4c shows an elastic moduli

comparison between SIPNs under two different states of stress: uniaxial and biaxial tensions; the solid bars correspond to those obtained by the uniaxial tensile, while the bars with a line pattern correspond to the biaxial tensile test. Here, it could be observed that the elastic moduli of the SIPNs under uniaxial and biaxial states of stress were similar regarding their respective polymeric composition. However, we found that the SIPNs2 and SIPNs3 exhibited almost two times lower elastic moduli than SIPNs1. Figure 4d can explain this result; it shows the influence of the SIPNs composition on their swelling behavior and its correlation with the elastic modulus. Hence, increasing the CS/PVA/GEN ratio produced an increment in the swelling capability but decreased the elastic modulus of the hydrated SIPNs. It must remain that the mechanical assays were conducted with hydrated membranes swollen at an equilibrium state. Hence, the water within the polymeric network can cause a pre-stress condition in the polymeric chains, limiting its elongation and mechanical strength. Therefore, the amount of water present in the polymer network directly affects the mechanical response of the polymeric chains [10, 83]. We found that the elasticity and strength were affected by the reduction of the PDMS; nonetheless, the surface and volume hydrophilicity behaviors of those SIPNs with less content of PDMS resulted in an attractive alternative for biological applications.

### 3.5 In vitro viability and cytotoxicity assays

Figure 5a–d depicts cell culture results on the SIPNs’ surface after 48 h. Here, the live and dead cells are shown in green and red colors, respectively. Our in-vitro viability and cytotoxicity results demonstrated a predomination of living cells on the SIPNs’ surfaces; therefore, any possible cytotoxicity effect is discarded. Now considering our performed image analysis, just a few dead cells were identified on the SIPNs or on the glass coverslips that were used as control material; therefore, we obtained cell viability of around 96%. Notice that in all cases, the cells cultured on the SIPNs exhibited predominant polygonal and fusiform shapes. The main difference between them was their size and number. The human fibroblasts cultured on SIPNs3 were smaller in size and fewer in number compared with SIPNs1 and SIPNs2. In accordance with previous studies, the polygonal and fusiform shape of cells indicates a favorable cell adhesion state and proliferation of them [31, 84, 85].

Figure 5e–h shows the cell counting results and their corresponding statistical distribution for the maximum length of the longitudinal cells’ axis (known as maximum Feret diameter). These results correspond to the image analyses performed after 48 h of cell culture. In Fig. 5e, we observed that cells cultured on the control material presented a Feret diameter distribution centered at  $74.18 \mu\text{m}$ , while the SIPNs1,

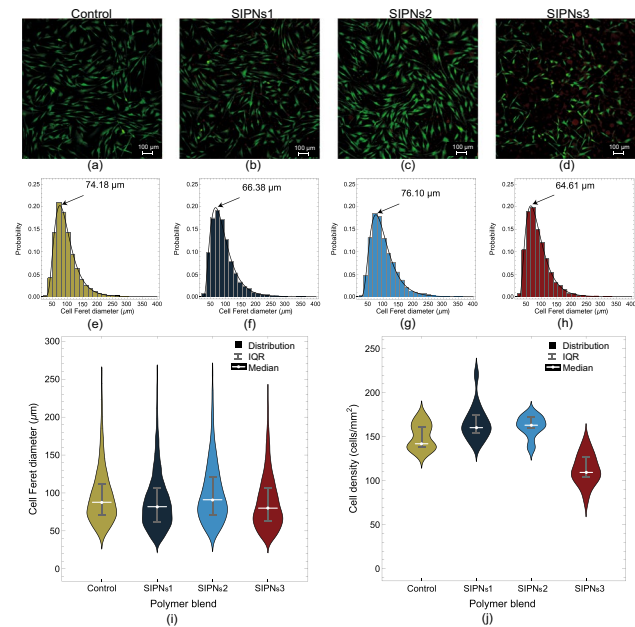


**Fig. 5** Cytotoxicity characterization and statistical distribution of live/dead assay by digital image analysis. **a–d** In vitro human BJ fibroblasts response to the SIPNs, after 48 h of culture, **e–h** Statistics distribution of Feret diameter of each SIPNs, **i** Violin charts representation of cells' Feret diameter distribution for each SIPNs, white center-line: median, whiskers: first and third quartile, **j** Violin charts representation of cell density distribution for each SIPNs, white center-line: median, whiskers: first and third quartile

SIPNs2, and SIPNs3 presented Feret diameter distributions centered at 66.38 μm, 76.1 μm, and 64.61 μm respectively (See Fig. 5f–h). According to the literature, human fibroblasts vary in size from 10 to 100 microns [86]; thus, based on this range of size, our SIPNs offer suitable conditions for this type of cell. Moreover, according to recent studies, cells with larger sizes correlate with better substrate adhesion and better collagen production, which is one of the main components of the extracellular matrix and is necessary for wound repairing [87–91].

As noted in the previous distribution charts (Fig. 5e–h), they show a positive skew; thus, the median and interquartile interval for the Feret diameter and cell density will be used to get a fair interpretation of the data. Figure 5i, j depicts further statistical analyses involving the cell morphology and the cellular density observed on the SIPNs. Figure 5i shows the Feret diameter distribution of SIPNs, including their median values (white line) and the interquartile range (IQR) in gray bars. The median Feret diameter values were 87.9 μm, 82.21 μm, 90.87 μm, and 80.15 μm and its IQR were 113.08–69.87 μm, 107.04–62.59 μm, 122.14–70.76 μm, and 107.36–61.48 μm for the control, SIPNs1, SIPNs2, and SIPNs3; respectively. Finally, Fig. 5j exhibits cell density distribution for control and each SIPNs. The white lines represent the median values of cell density. Thus, the median

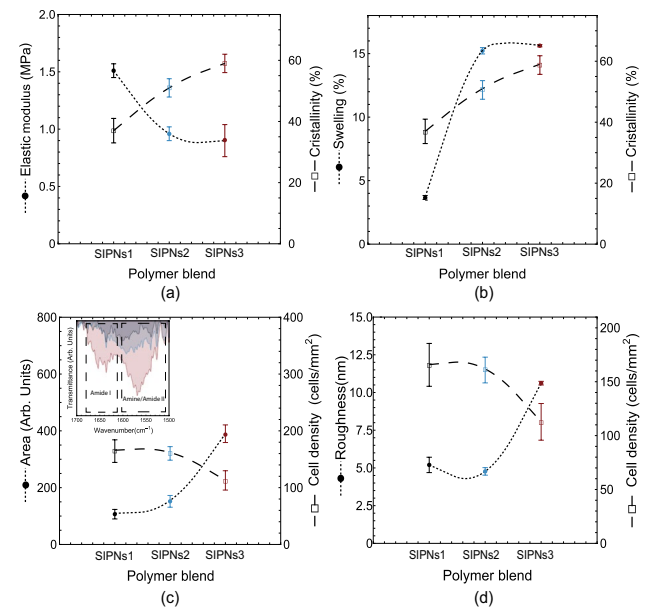


**Fig. 6** **a** Comparison between elastic modulus and crystallinity as a function of SIPNs, **b** correlation between swelling capability and crystallinity of SIPNs, **c** correlation of CS with the average number of cells per squared millimeter, **d** relation between roughness and the average values of cell density

values of the number of cells per square millimeter was 142.26, 160.41, 162.75, and 109.47 cells/mm<sup>2</sup>, and its IQR were 160.41–137.58 cells/mm<sup>2</sup>, 173.88–153.39 cells/mm<sup>2</sup>, 1172.12–158.07 cells/mm<sup>2</sup>, and 126.46–102.45 cells/mm<sup>2</sup> for control, SIPNs1, SIPNs2, and SIPNs3, respectively.

The cell density results for SIPNs1 and SIPNs2 were 13% and 14% higher than the control sample. The increase suggests a better fibroblast affinity for SIPNs1 and SIPNs2 than SIPNs3 or the control material. It can be observed from live/dead assay images from SIPNs1 and SIPNs2s that the fibroblasts covered almost all the surfaces. The cell sizes were more extensive than those cells seeded in the control material. Therefore, it indicates that SIPNs1 and SIPNs2 had better cell spreading and adhesion features than SIPNs3 or even the control material. Thus, based on our results, the SIPNs1 and SIPNs2 presented the best cell spreading and cell sizes; therefore, they possess great potential to be used in scaffolds for tissue engineering or wound healing applications.

### 3.6 Discussion

According to the literature, rigidity, volume hydrophilicity, chemical composition, and roughness can influence the cells' seeded behavior [57–59, 92] on a substrate. Therefore, a comparison between these results was carried out, and it is presented below for our SIPNs; see Fig. 6.

Figure 6a shows the relationship between the elastic modulus and the crystallinity percentage of our SIPNs. We found that the elastic modulus did not decrease as the crystallinity percentage did, increasing the CS/PVA/GEN ratio. This result is counterintuitive because polymers with higher crystallinities must offer higher elastic moduli when the polymers are tested in dry conditions. This counterintuitive result can be explained as follows: increasing the CS/PVA/GEN content will increase the quantity of free PVA chains within the polymeric network; these PVA chains will tend to fold, raising crystalline regions. Thus, the roughness and crystallinity percentage will also tend to increase; additionally, those SIPNs with higher content of PVA will present more swelling capacity, shown in Fig. 6b. Hence, samples with higher swelling capacity will trap more water into their polymer network, but their rigidity will decrease if they are mechanically tested under hydrated conditions, as observed in their mechanical response. (see Fig. 6a, b and Fig. 4d) We found that the swelling capability increased 4.1 times for SIPNs2 and 4.2 times for SIPNs3 concerning SIPNs1. In the case of crystallinity, the SIPNs2 and SIPNs3 showed an increment of 1.38 times and 1.59 times, respectively, concerning SIPNs1. Regarding the mentioned values of crystallinity, it was expected a higher swelling capacity of the SIPNs3; however, it was in the same range as the SIPNs2. It suggests that the PDMS polymer network might be limiting the expansion of PVA chains during the swelling process and, therefore, also limiting water absorption.

Figure 6c shows the relationship between the availability of CS N–H/OH functional groups and the cell density as a function of SIPNs composition. The availability of CS functional groups was calculated as the area under the curve for bands 1700–1800  $\text{cm}^{-1}$ . These bands correspond to amides I and amines/amides II (see Fig. 6c inset). These functional groups of CS are important because are similar to those that the glycosaminoglycans present in the extracellular matrix of the skin [28] and tend to enhance the viability of seeded cells. Figure 6c depicts an increment of CS functional groups as the CS/PVA/GEN ratio also increases; however, the cell density response presents an opposite behavior. It means that another parameter has an influence on the biological response. We found that the other parameter was the roughness of the SIPNs.

Figure 6d shows the dependence between surface roughness and the number of cells per square millimeter depending on the material composition. This figure demonstrates that as the CS/PVA/GEN ratio increases, the roughness also increases, whereas cell density decreases. Thus, higher random roughness on the surface of the SIPNs will imply a lower cell density response of the SIPNs. According to previous studies, the random surface roughness of the material might affect cell adhesion. Notice that our results were in accordance with the trend reported for other or similar

materials by different authors [57–61]. They reported similar values of roughness for which cultured human fibroblast showed good viability and adhesion features [57–59]. Therefore, we conclude that SIPNs1 and SIPNs2 can be considered potential materials for further developing scaffolds in tissue engineering or wound healing applications.

## 4 Conclusions

We demonstrated that semi-interpenetrating polymeric networks, varying the weight ratios of poly(dimethylsiloxane) and chitosan/poly(vinyl alcohol)/genipin, can be successfully obtained by using the solvent casting method. From AFM results, it was found that the SIPNs surface's roughness was increased twofold for PDMS/CS/PVA/GEN 3:7 weight ratio with respect to the PDMS/CS/PVA/GEN 7:3 weight ratio, suggesting that roughness values will be dominated for the polymer with higher concentration in the blend. The surface hydrophilicity results yield contact angles ranging between  $55^\circ$  and  $75^\circ$  which are values that will provide a proper human fibroblast adhesion for our SIPNs. Regarding the volume hydrophilicity, evaluated through the swelling capability, we found that volume hydrophilicity increased for those SIPNs with higher CS/PVA/GEN ratio content. It occurred due to the water affinity of free OH and  $\text{NH}_2$  groups of CS and PVA, which are in the SIPNs. Thus higher availability of free N–H/OH and  $\text{NH}_2$  groups will imply higher volume hydrophilicity, as the FT-IR and swelling results demonstrated it. Besides, the thermal and mechanical stability were tested. In this sense, The TGA results indicate that our SIPNs will be thermally stable until  $230^\circ\text{C}$ . This temperature is adequate if a thermal sterilization process is needed. Uniaxial and biaxial tensile assays were useful in evaluating the mechanical response of the SIPNs. Their elastic moduli were in the same order of magnitude, which was between 1 and 1.6 MPa. Thus, according to the cell density results, the rigidity of the SIPNs had no significant effect on the seeded fibroblast cells for SIPN1 and SIPN2. In contrast, the combinations of free N–H/OH groups of CS and PVA and the roughness for SIPN1 and SIPN2 significantly affected their cell spreading and cell density response. Thus, considering the physicochemical properties and biological behavior of the tested SIPNs, we found that SIPN1 and SIPN2 were the more suitable polymeric blends that could be potentially used for skin substitutes, wound healing/dressing, or as a scaffold for tissue engineering.

**Acknowledgements** This work was developed with the financial support from PAPIIT DGAPA-UNAM program through grant IN102421. J.A. Benítez-Martínez appreciates financial support from CONACyT during his Ph.D. studies. The authors are grateful to MSc. Adriana Tejada for X-Ray measurements, Eriseth Reyes Morales for TGA characterization, Carlos Flores for AFM microscopy, and Miguel Angel

Canseco for FT-IR measurements. The authors are grateful for the support and comments received from Prof. Mathieu Hautefeuille regarding the present work and the authors also thanks the Laboratorio Nacional de Soluciones Biomiméticas para Diagnóstico y Terapia for the technical support for obtaining micrographs with the Thunder microscope (CONACyT).

**Author Contributions** Conceptualization, JB, and FS; methodology, JB, AR, DP, AH; biological assays, AR and GV; formal analysis, FS, JB, IG, and GV; writing—original draft preparation, JB, IG, AR, and FS; writing—review and editing, FS, AH and IG; funding acquisition, FS.

**Funding** This study was funded by PAPIIT DGAPA-UNAM program through Grant IN102421.

**Availability of data and materials** Data are contained within the article.

**Code availability** Not applicable.

## Declarations

**Conflict of interest** The authors declare no conflict of interest.

**Ethics approval** Not applicable.

**Consent to participate** Not applicable.

**Consent for publication** All the authors have read and agreed to the published version of the manuscript.

**Open Access** This article is licensed under a Creative Commons Attribution 4.0 International License, which permits use, sharing, adaptation, distribution and reproduction in any medium or format, as long as you give appropriate credit to the original author(s) and the source, provide a link to the Creative Commons licence, and indicate if changes were made. The images or other third party material in this article are included in the article's Creative Commons licence, unless indicated otherwise in a credit line to the material. If material is not included in the article's Creative Commons licence and your intended use is not permitted by statutory regulation or exceeds the permitted use, you will need to obtain permission directly from the copyright holder. To view a copy of this licence, visit <http://creativecommons.org/licenses/by/4.0/>.

## References


1. J. Benítez-Martínez, I. Garnica-Palafox, G. Vázquez-Victorio, M. Hautefeuille, F. Sánchez-Arévalo, Semi-interpenetrating polymeric networks based on poly (dimethylsiloxane)-chitosan-poly (vinyl alcohol) crosslinked with genipin with possible use in biomedical applications. *J. Mater. Sci.* **56**(9), 5936–5955 (2021). <https://doi.org/10.1007/s10853-020-05683-3>
2. N. Vázquez, F. Sánchez-Arévalo, A. Maciel-Cerda, I. Garnica-Palafox, R. Ontiveros-Tlachi, C. Chaires-Rosas, G. Piñón-Zarate, M. Herrera-Enríquez, M. Hautefeuille, R. Vera-Graziano, A. Castell-Rodríguez, Influence of the PLGA/gelatin ratio on the physical, chemical and biological properties of electrospun scaffolds for wound dressings. *Biomed. Mater.* **14**(4), 045006 (2019). <https://doi.org/10.1088/1748-605x/ab1741>
3. W.H. Organization, Diabetes. <https://www.who.int/news-room/fact-sheets/detail/diabetes>. Accessed 27 Feb 2023 (2022)
4. R.G. Frykberg, J. Banks, Challenges in the treatment of chronic wounds. *Adv. Wound Care* **4**(9), 560–582 (2015). <https://doi.org/10.1089/wound.2015.0635>. (PMID: 26339534)
5. A.D. Metcalfe, M.W.J. Ferguson, Tissue engineering of replacement skin: the crossroads of biomaterials, wound healing, embryonic development, stem cells and regeneration. *J. R. Soc. Interface* **4**(14), 413–437 (2007). <https://doi.org/10.1098/rsif.2006.0179>
6. C. Ghobril, M.W. Grinstaff, The chemistry and engineering of polymeric hydrogel adhesives for wound closure: a tutorial. *Chem. Soc. Rev.* **44**, 1820–1835 (2015). <https://doi.org/10.1039/C4CS00332B>
7. V.N.V.A. Uppuluri, S.T. Sathanantham, S.K. Bhimavarapu, L. Elumalai, Polymeric hydrogel scaffolds: skin tissue engineering and regeneration. *Adv. Pharm. Bull.* **12**(3), 437 (2022)
8. L. Ma, C. Gao, Z. Mao, J. Zhou, J. Shen, X. Hu, C. Han, Collagen/chitosan porous scaffolds with improved biostability for skin tissue engineering. *Biomaterials* **24**(26), 4833–4841 (2003). [https://doi.org/10.1016/S0142-9612\(03\)00374-0](https://doi.org/10.1016/S0142-9612(03)00374-0)
9. S. Tavakoli, A.S. Klar, Bioengineered skin substitutes: advances and future trends. *Appl. Sci.* (2021). <https://doi.org/10.3390/app11041493>
10. N.A. Peppas, A.S. Hoffman, 1.3.2E Hydrogels, in *Biomaterials Science (Fourth Edition)*, 4th edn., ed. by W.R. Wagner, S.E. Sakiyama-Elbert, G. Zhang, M.J. Yaszemski (Academic Press, San Diego, 2020), pp.153–166. <https://doi.org/10.1016/B978-0-12-816137-1.00014-3>
11. D.M. Supp, S.T. Boyce, Engineered skin substitutes: practices and potentials. *Clin. Dermatol.* **23**(4), 403–412 (2005). <https://doi.org/10.1016/j.clindermatol.2004.07.023>
12. M. Varkey, J. Ding, E.E. Tredget, Advances in skin substitutes-potential of tissue engineered skin for facilitating anti-fibrotic healing. *J. Funct. Biomater.* **6**(3), 547–563 (2015). <https://doi.org/10.3390/jfb6030547>
13. C. Dai, S. Shih, A. Khachemoune, Skin substitutes for acute and chronic wound healing: an updated review. *J. Dermatolog. Treat.* (2020). <https://doi.org/10.1080/09546634.2018.1530443>. (PMID: 30265595)
14. M.N. Nicholas, M.G. Jeschke, S. Amini-Nik, Methodologies in creating skin substitutes. *Cell. Mol. Life Sci.* **73**(18), 3453–3472 (2016)
15. M. Sheikholeslam, M.E.E. Wright, M.G. Jeschke, S. Amini-Nik, Biomaterials for skin substitutes. *Adv. Healthc. Mater.* **7**(5), 1700897 (2018). <https://doi.org/10.1002/adhm.201700897>
16. M.I. Baker, S.P. Walsh, Z. Schwartz, B.D. Boyan, A review of polyvinyl alcohol and its uses in cartilage and orthopedic applications. *J. Biomed. Mater. Res. B Appl. Biomater.* **100B**(5), 1451–1457 (2012). <https://doi.org/10.1002/jbm.b.32694>
17. M.M. Pillai, V. Elakkiya, H. LakshmiPriya, J. Gopinathan, R. Selvakumar, A. Bhattacharyya, A novel method for developing three dimensional (3d) silk-PVA microenvironments for bone tissue engineering-an in vitro study. *Biomed. Phys. Eng. Express* **4**(2), 027006 (2018)
18. N.A. Peppas, E.W. Merrill, Development of semicrystalline poly(vinyl alcohol) hydrogels for biomedical applications. *J. Biomed. Mater. Res.* **11**(3), 423–434 (1977). <https://doi.org/10.1002/jbm.820110309>
19. I.M. Garnica-Palafox, F.M. Sánchez-Arévalo, Influence of natural and synthetic crosslinking reagents on the structural and mechanical properties of chitosan-based hybrid hydrogels. *Carbohydr. Polym.* **151**, 1073–1081 (2016). <https://doi.org/10.1016/j.carbpol.2016.06.036>
20. V.M. Bispo, A.A. Mansur, E.F. Barbosa-Stancioli, H.S. Mansur, Biocompatibility of nanostructured chitosan/poly (vinyl alcohol) blends chemically crosslinked with genipin for biomedical applications. *J. Biomed. Nanotechnol.* **6**(2), 166–175 (2010)

21. E.S. Costa-Júnior, E.F. Barbosa-Stancioli, A.A.P. Mansur, W.L. Vasconcelos, H.S. Mansur, Preparation and characterization of chitosan/poly(vinyl alcohol) chemically crosslinked blends for biomedical applications. *Carbohydr. Polym.* **76**(3), 472–481 (2009). <https://doi.org/10.1016/j.carbpol.2008.11.015>
22. H.M.P. Naveen Kumar, M.N. Prabhakar, C. Venkata Prasad, K. Madhusudhan Rao, T.V. Ashok Kumar Reddy, K. Chowdoji Rao, M.C.S. Subha, Compatibility studies of chitosan/PVA blend in 2% aqueous acetic acid solution at 30 °C. *Carbohydr. Polym.* **82**(2), 251–255 (2010). <https://doi.org/10.1016/j.carbpol.2010.04.021>
23. F. Croisier, C. Jérôme, Chitosan-based biomaterials for tissue engineering. *Eur. Polym. J.* **49**(4), 780–792 (2013). <https://doi.org/10.1016/j.eurpolymj.2012.12.009>. **(Biobased Polymers and Related Materials)**
24. M.O.G. Ferreira, L.L.R. Leite, I.S. de Lima, H.M. Barreto, L.C.C. Nunes, A.B. Ribeiro, J.A. Osajima, E.C. da Silva Filho, Chitosan hydrogel in combination with nerolidol for healing wounds. *Carbohydr. Polym.* **152**, 409–418 (2016). <https://doi.org/10.1016/j.carbpol.2016.07.037>
25. R. Jayakumar, M. Prabaharan, P.S. Kumar, S. Nair, H. Tamura, Biomaterials based on chitin and chitosan in wound dressing applications. *Biotechnol. Adv.* **29**(3), 322–337 (2011)
26. H. Liu, C. Wang, C. Li, Y. Qin, Z. Wang, F. Yang, Z. Li, J. Wang, A functional chitosan-based hydrogel as a wound dressing and drug delivery system in the treatment of wound healing. *RSC Adv.* **8**, 7533–7549 (2018). <https://doi.org/10.1039/C7RA13510F>
27. A. Moeini, P. Pedram, P. Makvandi, M. Malinconico, G.G. d'Ayala, Wound healing and antimicrobial effect of active secondary metabolites in chitosan-based wound dressings: a review. *Carbohydr. Polym.* **233**, 115839 (2020). <https://doi.org/10.1016/j.carbpol.2020.115839>
28. M.-C. Yang, S.-S. Wang, N.-K. Chou, N.-H. Chi, Y.-Y. Huang, Y.-L. Chang, M.-J. Shieh, T.-W. Chung, The cardiomyogenic differentiation of rat mesenchymal stem cells on silk fibroin-polysaccharide cardiac patches in vitro. *Biomaterials* **30**(22), 3757–3765 (2009). <https://doi.org/10.1016/j.biomaterials.2009.03.057>
29. M.F. Butler, Y.-F. Ng, P.D.A. Pudney, Mechanism and kinetics of the crosslinking reaction between biopolymers containing primary amine groups and genipin. *J. Polym. Sci. Part A Polym. Chem.* **41**(24), 3941–3953 (2003). <https://doi.org/10.1002/pola.10960>
30. I.M. Garnica-Palafox, F.M. Sánchez-Arévalo, C. Velasquillo, Z.Y. García-Carvajal, J. García-López, C. Ortega-Sánchez, C. Ibarra, G. Luna-Bárcenas, L. Solís-Arrieta, Mechanical and structural response of a hybrid hydrogel based on chitosan and poly(vinyl alcohol) cross-linked with epichlorohydrin for potential use in tissue engineering. *J. Biomater. Sci. Polym. Ed.* **25**(1), 32–50 (2014). <https://doi.org/10.1080/09205063.2013.833441>. (PMID: 24007370)
31. I.M. Garnica-Palafox, H.O. Estrella-Monroy, N.A. Vázquez-Torres, M. Álvarez-Camacho, A.E. Castell-Rodríguez, F.M. Sánchez-Arévalo, Influence of multi-walled carbon nanotubes on the physico-chemical and biological responses of chitosan-based hybrid hydrogels. *Carbohydr. Polym.* **236**, 115971 (2020). <https://doi.org/10.1016/j.carbpol.2020.115971>
32. R. Nathoo, N. Howe, G. Cohen, Skin substitutes: an overview of the key players in wound management. *J. Clin. Aesthet. Dermatol.* **7**(10), 44 (2014)
33. H. Debels, M. Hamdi, K. Abberton, W. Morrison, Dermal matrices and bioengineered skin substitutes: a critical review of current options. *Plast. Reconstr. Surg. Glob. Open* **3**(1), e284 (2015). <https://doi.org/10.1097/GOX.0000000000000219>
34. F. Ataollahi, S. Pramanik, A. Moradi, A. Dalilotojari, B. Pingguan-Murphy, W.A.B. Wan Abas, N.A. Abu Osman, Endothelial cell responses in terms of adhesion, proliferation, and morphology to stiffness of polydimethylsiloxane elastomer substrates. *J. Biomed. Mater. Res. Part A* **103**(7), 2203–2213 (2015). <https://doi.org/10.1002/jbm.a.35186>
35. N. Varshney, A.K. Sahi, K.Y. Vajanthri, S. Poddar, C.K. Balavigneswaran, A. Prabhakar, V. Rao, S.K. Mahto, Culturing melanocytes and fibroblasts within three-dimensional macroporous PDMS scaffolds: towards skin dressing material. *Cytotechnology* **71**(1), 287–303 (2019)
36. M. Morales-Hurtado, X. Zeng, P. Gonzalez-Rodriguez, J.E. Ten Elshof, E. van der Heide, A new water absorbable mechanical epidermal skin equivalent: the combination of hydrophobic PDMS and hydrophilic PVA hydrogel. *J. Mech. Behav. Biomed. Mater.* **46**, 305–317 (2015)
37. H.-W. Leung, Ecotoxicology of glutaraldehyde: Review of environmental fate and effects studies. *Ecotoxicol. Environ. Saf.* **49**(1), 26–39 (2001). <https://doi.org/10.1006/eesa.2000.2031>
38. I.C. Carvalho, H.S. Mansur, Engineered 3d-scaffolds of photo-crosslinked chitosan-gelatin hydrogel hybrids for chronic wound dressings and regeneration. *Mater. Sci. Eng. C* **78**, 690–705 (2017). <https://doi.org/10.1016/j.msec.2017.04.126>
39. F.S. Tenório, T.L. do Amaral Montanheiro, A.M.I. dos Santos, M. dos Santos Silva, A.P. Lemes, D.B. Tada, Chitosan hydrogel covalently crosslinked by gold nanoparticle: eliminating the use of toxic crosslinkers. *J. Appl. Polym. Sci.* **138**(6), 49819 (2021). <https://doi.org/10.1002/app.49819>
40. J. Chen, H. Yang, J. Li, J. Chen, Y. Zhang, X. Zeng, The development of an artificial skin model and its frictional interaction with wound dressings. *J. Mech. Behav. Biomed. Mater.* **94**, 308–316 (2019). <https://doi.org/10.1016/j.jmbbm.2019.03.013>
41. H.M.P. Naveen Kumar, M.N. Prabhakar, C. Venkata Prasad, K. Madhusudhan Rao, T.V. Ashok Kumar Reddy, K. Chowdoji Rao, M.C.S. Subha, Compatibility studies of chitosan/PVA blend in 2% aqueous acetic acid solution at 30 °C. *Carbohydr. Polym.* **82**(2), 251–255 (2010)
42. P.-Y. Zhuang, Y.-L. Li, L. Fan, J. Lin, Q.-L. Hu, Modification of chitosan membrane with poly(vinyl alcohol) and biocompatibility evaluation. *Int. J. Biol. Macromol.* **50**(3), 658–663 (2012). <https://doi.org/10.1016/j.ijbiomac.2012.01.026>
43. M.D. Figueroa-Pizano, I. Vélaz, F.J. Penas, P. Zavala-Rivera, A.J. Rosas-Durazo, A.D. Maldonado-Arce, M.E. Martínez-Barbosa, Effect of freeze-thawing conditions for preparation of chitosan-poly (vinyl alcohol) hydrogels and drug release studies. *Carbohydr. Polym.* **195**, 476–485 (2018). <https://doi.org/10.1016/j.carbpol.2018.05.004>
44. Y.P. Zheng, Y.K.C. Choi, K. Wong, S. Chan, A.F.T. Mak, Biomechanical assessment of plantar foot tissue in diabetic patients using an ultrasound indentation system. *Ultrasound Med. Biol.* **26**(3), 451–456 (2000). [https://doi.org/10.1016/S0301-5629\(99\)00163-5](https://doi.org/10.1016/S0301-5629(99)00163-5)
45. M. Mooney, A theory of large elastic deformation. *J. Appl. Phys.* **11**(9), 582–592 (1940). <https://doi.org/10.1063/1.1712836>
46. N. Kumar, V.V. Rao, Hyperelastic Mooney-Rivlin model: determination and physical interpretation of material constants. *Parameters* **2**(10), 01 (2016)
47. Y. Dong, R. Lin, D. Bhattacharyya, Determination of critical material parameters for numerical simulation of acrylic sheet forming. *J. Mater. Sci.* **40**(2), 399–410 (2005)
48. I. Garnica-Palafox, M. Álvarez-Camacho, F. Sánchez-Arévalo, Macro- and micromechanical responses of an elastomeric membrane undergoing biaxial tension by indentation. *J. Mater. Sci.* **54**(22), 14255–14274 (2019)
49. K.M. McGee, M.K. Vartiainen, P.T. Khaw, R. Treisman, M. Bailly, Nuclear transport of the serum response factor coactivator mrtf-a is downregulated at tensional homeostasis. *EMBO Rep.* **12**(9), 963–970 (2011). <https://doi.org/10.1038/embor.2011.141>

50. C. Djerassi, J.D. Gray, F.A. Kincl, Naturally occurring oxygen heterocyclics. ix.1 isolation and characterization of genipin2. *J. Org. Chem.* **25**(12), 2174–2177 (1960). <https://doi.org/10.1021/jo01082a022>
51. L.H. Sperling, V. Mishra, The current status of interpenetrating polymer networks. *Polym. Adv. Technol.* **7**(4), 197–208 (1996)
52. R.S. Marques, T.C.O. Mac Leod, I.V.P. Yoshida, V. Mano, M.D. Assis, M.A. Schiavon, Synthesis and characterization of semi-interpenetrating networks based on poly(dimethylsiloxane) and poly(vinyl alcohol). *J. Appl. Polym. Sci.* **115**(1), 158–166 (2010). <https://doi.org/10.1002/app.31006>
53. E.C. Coelho, D.P. dos Santos, K.J. Ciuffi, J.L. Ferrari, B.A. Ferreira, M.A. Schiavon, Poly(vinyl alcohol) and poly(dimethylsiloxane)-based interpenetrating polymer networks via radical polymerisation. *J. Polym. Res.* **21**(9), 561 (2014). <https://doi.org/10.1007/s10965-014-0561-x>
54. A. Oláh, H. Hillborg, G.J. Vancso, Hydrophobic recovery of UV/ozone treated poly (dimethylsiloxane): adhesion studies by contact mechanics and mechanism of surface modification. *Appl. Surf. Sci.* **239**(3–4), 410–423 (2005)
55. R.N. Palchesko, L. Zhang, Y. Sun, A.W. Feinberg, Development of polydimethylsiloxane substrates with tunable elastic modulus to study cell mechanobiology in muscle and nerve. *PLoS One* **7**(12), 51499 (2012)
56. S. Prauzner-Bechcicki, J. Raczkowska, E. Madej, J. Pabijan, J. Lukes, J. Sepitka, J. Rysz, K. Awsiuk, A. Bernasik, A. Budkowski et al., PDMS substrate stiffness affects the morphology and growth profiles of cancerous prostate and melanoma cells. *J. Mech. Behav. Biomed. Mater.* **41**, 13–22 (2015)
57. A.S. Crouch, D. Miller, K.J. Luebke, W. Hu, Correlation of anisotropic cell behaviors with topographic aspect ratio. *Biomaterials* **30**(8), 1560–1567 (2009). <https://doi.org/10.1016/j.biomaterials.2008.11.041>
58. A. Ranella, M. Barberoglou, S. Bakogianni, C. Fotakis, E. Stratikis, Tuning cell adhesion by controlling the roughness and wettability of 3d micro/nano silicon structures. *Acta Biomater.* **6**(7), 2711–2720 (2010). <https://doi.org/10.1016/j.actbio.2010.01.016>
59. S. Fiejdasz, W. Horak, J. Lewandowska-Lancucka, M. Szuwarzynski, J. Salwinski, M. Nowakowska, Tuning of elasticity and surface properties of hydrogel cell culture substrates by simple chemical approach. *J. Colloid Interface Sci.* **524**, 102–113 (2018). <https://doi.org/10.1016/j.jcis.2018.04.004>
60. K. Anselme, M. Bigerelle, B. Noel, E. Dufresne, D. Judas, A. Iost, P. Hardouin, Qualitative and quantitative study of human osteoblast adhesion on materials with various surface roughnesses. *J. Biomed. Mater. Res.* **49**(2), 155–166 (2000)
61. M. Ball, D.M. Grant, W.-J. Lo, C.A. Scotchford, The effect of different surface morphology and roughness on osteoblast-like cells. *J. Biomed. Mater. Res. Part A* **86A**(3), 637–647 (2008). <https://doi.org/10.1002/jbm.a.31652>
62. S. Gupta, T.J. Webster, A. Sinha, Evolution of PVA gels prepared without crosslinking agents as a cell adhesive surface. *J. Mater. Sci. Mater. Med.* **22**(7), 1763–1772 (2011). <https://doi.org/10.1007/s10856-011-4343-2>
63. J.N. Lee, C. Park, G.M. Whitesides, Solvent compatibility of poly (dimethylsiloxane)-based microfluidic devices. *Anal. Chem.* **75**(23), 6544–6554 (2003)
64. I.M. Garnica-Palafox, H.O. Estrella-Monroy, J.A. Benítez-Martínez, M. Bizarro, F.M. Sánchez-Arévalo, Influence of genipin and multi-walled carbon nanotubes on the dye capture response of CS/PVA hybrid hydrogels. *J. Polym. Environ.* (2022). <https://doi.org/10.1007/s10924-022-02534-x>
65. E.A. El-Hefian, M.M. Nasef, A.H. Yahaya, The preparation and characterization of chitosan/poly (vinyl alcohol) blended films. *E-J. Chem.* **7**(4), 1212–1219 (2010). <https://doi.org/10.1155/2010/626235>
66. Y. Xie, L. Wang, Y. Zhang, H. Li, R. Huang, An in situ silicone-silicone interpenetrating polymer network (ipn) with higher mechanical property, higher hydrophilicity, and lower protein adsorption. *J. Mater. Sci.* **53**(12), 9325–9339 (2018). <https://doi.org/10.1007/s10853-018-2146-2>
67. J.A. Juárez-Moreno, A. Ávila-Ortega, A.I. Oliva, F. Avilés, J.V. Cauich-Rodríguez, Effect of wettability and surface roughness on the adhesion properties of collagen on PDMS films treated by capacitively coupled oxygen plasma. *Appl. Surf. Sci.* **349**, 763–773 (2015). <https://doi.org/10.1016/j.apsusc.2015.05.063>
68. A. Salati, H. Keshvari, A. Karkhaneh, S. Taranejoo, Design and fabrication of artificial skin: Chitosan and gelatin immobilization on silicone by poly acrylic acid graft using a plasma surface modification method. *J. Macromol. Sci. Part B* **50**(10), 1972–1982 (2011). <https://doi.org/10.1080/00222348.2010.549438>
69. K. Lewandowska, Miscibility and thermal stability of poly (vinyl alcohol)/chitosan mixtures. *Thermochim. Acta* **493**(1–2), 42–48 (2009)
70. G. Camino, S.M. Lomakin, M. Lazzari, Polydimethylsiloxane thermal degradation part I. Kinetic aspects. *Polymer* **42**(6), 2395–2402 (2001). [https://doi.org/10.1016/S0032-3861\(00\)00652-2](https://doi.org/10.1016/S0032-3861(00)00652-2)
71. R. Pimentel-Domínguez, A.M. Velázquez-Benítez, J.R. Vélez-Cordero, M. Hautefeuille, F. Sánchez-Arévalo, J. Hernández-Cordero, Photothermal effects and applications of polydimethylsiloxane membranes with carbon nanoparticles. *Polymers* (2016). <https://doi.org/10.3390/polym8040084>
72. Z. Dai, J. Ronholm, Y. Tian, B. Sethi, X. Cao, Sterilization techniques for biodegradable scaffolds in tissue engineering applications. *J. Tissue Eng.* **7**, 2041731416648810 (2016). <https://doi.org/10.1177/2041731416648810>. (PMID: 27247758)
73. P.-A. Albouy, The conformation of poly(dimethylsiloxane) in the crystalline state. *Polymer* **41**(8), 3083–3086 (2000). [https://doi.org/10.1016/S0032-3861\(99\)00664-3](https://doi.org/10.1016/S0032-3861(99)00664-3)
74. L. Qu, G. Huang, Q. Wang, Z. Xie, Effect of diphenylsiloxane unit content on aggregation structure of poly(dimethylsiloxane-co-diphenylsiloxane). *J. Polym. Sci. Part B Polym. Phys.* **46**(1), 72–79 (2008). <https://doi.org/10.1002/polb.21343>
75. G.L. Jadav, V.K. Aswal, H. Bhatt, J.C. Chaudhari, P.S. Singh, Influence of film thickness on the structure and properties of PDMS membrane. *J. Membr. Sci.* **415–416**, 624–634 (2012). <https://doi.org/10.1016/j.memsci.2012.05.043>
76. F.M. Sánchez-Arévalo, I.M. Garnica-Palafox, P. Jagdale, J. Hernández-Cordero, S.E. Rodil, A.O. Okonkwo, F.C.R. Hernandez, A. Tagliaferro, Photomechanical response of composites based on PDMS and carbon soot nanoparticles under IR laser irradiation. *Opt. Mater. Express* **5**(8), 1792–1805 (2015). <https://doi.org/10.1364/OME.5.001792>
77. E. Mogilevskaya, T. Akopova, A. Zelenetskii, A. Ozerin, The crystal structure of chitin and chitosan. *Polym. Sci. Ser. A* **48**(2), 116–123 (2006)
78. D. Depan, B. Kumar, R.P. Singh, Preparation and characterization of novel hybrid of chitosan-g-PDMS and sodium montmorillonite. *J. Biomed. Mater. Res. B Appl. Biomater.* **84B**(1), 184–190 (2008). <https://doi.org/10.1002/jbm.b.30860>
79. C.-H. Chen, F.-Y. Wang, C.-F. Mao, C.-H. Yang, Studies of chitosan. i. Preparation and characterization of chitosan/poly(vinyl alcohol) blend films. *J. Appl. Polym. Sci.* **105**(3), 1086–1092 (2007). <https://doi.org/10.1002/app.26257>
80. C.-H. Chen, F.-Y. Wang, C.-F. Mao, W.-T. Liao, C.-D. Hsieh, Studies of chitosan: ii. preparation and characterization of chitosan/poly(vinyl alcohol)/gelatin ternary blend films. *Int. J. Biol. Macromol.* **43**(1), 37–42 (2008). <https://doi.org/10.1016/j.ijbio mac.2007.09.005>. (10th International Conference on Chitin and Chitosan)
81. D.S. Kim, V. Dhand, K.Y. Rhee, S.-J. Park, Study on the effect of silanization and improvement in the tensile behavior of

- graphene-chitosan-composite. *Polymers* **7**(3), 527–551 (2015). <https://doi.org/10.3390/polym7030527>
82. C. Li, M. She, X. She, J. Dai, L. Kong, Functionalization of polyvinyl alcohol hydrogels with graphene oxide for potential dye removal. *J. Appl. Polym. Sci.* (2014). <https://doi.org/10.1002/app.39872>
  83. P. Flory et al., *Principles of Polymer Chemistry Ithaca* (Cornell University, NY, 1953)
  84. J. Vivas, D. Garzón-Alvarado, M. Cerrolaza, Modeling cell adhesion and proliferation: a cellular-automata based approach. *Adv. Model. Simul. Eng. Sci.* **2**(1), 32 (2015)
  85. M. Imaninezhad, J. Schober, D. Griggs, P. Ruminski, I. Kuljanishvili, S.P. Zustiak, Cell attachment and spreading on carbon nanotubes is facilitated by integrin binding. *Front. Bioeng. Biotechnol.* **6**, 129 (2018). <https://doi.org/10.3389/fbioe.2018.00129>
  86. E.J. Chong, T.T. Phan, I.J. Lim, Y.Z. Zhang, B.H. Bay, S. Ramakrishna, C.T. Lim, Evaluation of electrospun PCL/gelatin nanofibrous scaffold for wound healing and layered dermal reconstitution. *Acta Biomater.* **3**(3), 321–330 (2007). <https://doi.org/10.1016/j.actbio.2007.01.002>. (2nd TMS Symposium on biological materials science)
  87. G.J. Fisher, Y. Shao, T. He, Z. Qin, D. Perry, J.J. Voorhees, T. Quan, Reduction of fibroblast size/mechanical force down-regulates  $\text{tgf-}\beta$  type ii receptor: implications for human skin aging. *Aging Cell* **15**(1), 67–76 (2016). <https://doi.org/10.1111/accel.12410>
  88. J.-W. Shin, S.-H. Kwon, J.-Y. Choi, J.-I. Na, C.-H. Huh, H.-R. Choi, K.-C. Park, Molecular mechanisms of dermal aging and antiaging approaches. *Int. J. Mol. Sci.* (2019). <https://doi.org/10.3390/ijms20092126>
  89. G. Shabestani Monfared, P. Ertl, M. Rothbauer, An on-chip wound healing assay fabricated by xurography for evaluation of dermal fibroblast cell migration and wound closure. *Sci. Rep.* **10**(1), 1–14 (2020)
  90. Z. Yu, M.J. Smith, R.C.M. Siow, K.-K. Liu, Ageing modulates human dermal fibroblast contractility: quantification using nano-biomechanical testing. *Biochim. Biophys. Acta (BBA) Mol. Cell Res.* **1868**(5), 118972 (2021). <https://doi.org/10.1016/j.bbamcr.2021.118972>
  91. Y. Xiang, Z. Qin, Y. Yang, G.J. Fisher, T. Quan, Age-related elevation of HGF is driven by the reduction of fibroblast size in a  $\text{yap/taz/ccn2}$  axis-dependent manner. *J. Dermatol. Sci.* **102**(1), 36–46 (2021). <https://doi.org/10.1016/j.jdermsci.2021.02.003>
  92. L. Gao, H. Gan, Z. Meng, R. Gu, Z. Wu, L. Zhang, X. Zhu, W. Sun, J. Li, Y. Zheng, G. Dou, Effects of genipin cross-linking of chitosan hydrogels on cellular adhesion and viability. *Colloids Surf. B* **117**, 398–405 (2014). <https://doi.org/10.1016/j.colsurfb.2014.03.002>

## Authors and Affiliations

Jorge Alejandro Benítez-Martínez<sup>1,2</sup> · Itzel Marisol Garnica-Palafox<sup>1</sup> · Adriana Rodríguez-Hernández<sup>3</sup> · Daniel Pérez-Calixto<sup>3,4</sup> · Genaro Vázquez-Victorio<sup>3</sup> · Agileo Hernández-Gordillo<sup>1</sup> · Francisco Manuel Sánchez-Arévalo<sup>1</sup> 

✉ Francisco Manuel Sánchez-Arévalo  
fsanchez@iim.unam.mx

Jorge Alejandro Benítez-Martínez  
jbenitez1393@gmail.com

Itzel Marisol Garnica-Palafox  
marisol.garnica@gmail.com

Adriana Rodríguez-Hernández  
adriana.rodriguez@ciencias.unam.mx

Daniel Pérez-Calixto  
daniel\_perez@ciencias.unam.mx

Genaro Vázquez-Victorio  
genvazquez@ciencias.unam.mx

Agileo Hernández-Gordillo  
agileohg@materiales.unam.mx

<sup>1</sup> Instituto de Investigaciones en Materiales, Universidad Nacional Autónoma de México, Cd. Universitaria, 04510 Mexico City, Mexico

<sup>2</sup> Posgrado en Ciencia e Ingeniería de Materiales, Universidad Nacional Autónoma de México, Cd. Universitaria, 04510 Mexico City, Mexico

<sup>3</sup> Laboratorio de micro y nanofabricación, Facultad de Ciencias, Depto. de Física, Universidad Nacional Autónoma de México, Cd. Universitaria, 04510 Mexico City, Mexico

<sup>4</sup> Subdirección de Genómica Poblacional, Instituto Nacional de Medicina Genómica, Periférico Sur No. 4809, Col. Arenal Tepepan, 1461 Mexico City, Mexico